Establishing Parameter Values for the Stone Erosion Process

Igor Barros Barbosa[1], Kidane Fanta Gebremariam[2] Panagiotis Perakis[1], Christian Schellewald[1], and Theoharis Theoharis[1]

[1] Department of Computer and Information Science, Norwegian University of Science and Technology (NTNU), Sem Sælands Vei 9, 7491, Trondheim, Norway
[2] Department of Chemistry, Norwegian University of Science and Technology (NTNU), Høgskoleringen 5, 7491, Trondheim, Norway

Abstract. The computer simulation of the naturally occurring stone erosion process is very attractive because it could enable us to predict the future state of important cultural heritage monuments based on different environment scenarios and thus allow us to take appropriate action in good time. This paper describes the design and construction of two automatic erosion chambers that allows to simulate the Salt and Freeze-and-Thaw effects respectively on a low budget, based on a control system using off-the-shelf components. It also details the parameters that are being measured after each erosion cycle (3D scan, electron microscopy, micro computed tomography, 3D microscopy, XRD and petrography) which will eventually lead to a publicly available database for erosion benchmarking. In the current phase we are only concentrating on Pentelic marble and two types of Grytdal soapstone. This work forms part of the PRESIOUS EU project (www.presious.eu).

Keywords: Cultural Heritage, Accelerated Erosion Chambers, Erosion Benchmarking.

1 Introduction

The purpose of our study is to contribute to the simulation of the fundamental and most common degradation mechanisms that impact objects that are built out of stone. Our ultimate aim is to model and simulate the physico-chemical processes that lead to the degradation of the stone-material of Cultural Heritage (CH) objects over time. Towards this aim we are on a course to implement a prototype for the mesh alteration that currently acts on the surface geometry and allows therefore to imitate manifestations of stone degradation phenomena like surface recession and crust formation.

We first revisit the definitions of the terms that are often used when the deterioration of stone is described. In general we distinguish the terms erosion and weathering based on the involved material movement. Erosion involves the exposure of stones to external forces and transport processes that originate from water or wind flow and gravity. Note that this also includes forces and transport processes due to ice, snow or waves. In contrast weathering denotes the

processes that are weakening or loosening stone particles internally. Beside the disintegration of stone into smaller pieces, weathering also involves the dissolution of material into water due to the effects of atmosphere and hydrosphere. However the terms erosion, weathering, decay, degradation and deterioration are used differently and interchangeably within different disciplines (Doehne & Price 2010). For more strict definitions refer to the ICOMOS-ISCS "Illustrated Glossary on Stone Deterioration Patterns" (Vergès-Belmin 2008).

The three main weathering processes which often work simultaneously to decompose rocks are *physical/mechanical*, *chemical* and *biological* in nature. One of the main causes of stone decay is the interaction between water and the porous structure. Water absorption can induce weathering on stone materials in several ways:

1. by **chemical reaction** with industrial pollutants mainly the atmospheric gases of carbon dioxide CO_2, sulfur dioxide SO_2 and nitrogen dioxide NO_2, that decay the stone material by changing its chemical composition;
2. by a physical mechanism through **mechanical stresses** due to freeze/thaw and wet/dry cycles, that disintegrate stones into smaller particles, which then can be removed by gravity, wind, water or ice;
3. by acting as a transport medium for **salts** in dissolution and recrystallization processes within the pore space;
4. by providing an essential substrate for **biological growth** of living organisms such as bacteria, fungi, algae and lichens.

Stone decay appears in many different forms. Stone may gradually and slowly weather away, leaving a solid surface behind. At other times sheets or flakes break off from the stone at once. Sometimes the surface starts to show blisters or a stone just loses its integrity and crumbles away. Some of the stones can appear perfectly intact for a long time while already losing cohesion underneath.

The two different chemical weathering scenarios that are usually distinguished are the weathering within a natural environment and the weathering within a polluted environment. The first (unpolluted) scenario considers (beside the air) only the gas carbon dioxide (CO_2), while the second scenario contains also the industrial gases sulfur and nitrogen dioxide (SO_2 and NO_2). The chemical weathering results in two main effects; the gain or loss of material. The first one is mostly visible as crust building up on surfaces, while the second one relates in most cases to surface recession. The crust formation is usually due to the deposition of chemical material in polluted environments, while the loss of material results mainly due to reactions of water with the stone-material and pollution gases. The chemical products in this process are subsequently washed away. Temperature and humidity play crucial roles in these processes.

The two different mechanical weathering scenarios that are usually distinguished are the weathering caused by soluble salts and the weathering caused by wet/dry and freeze/thaw cycles. Along with air pollution, soluble salts represent one of the most important causes of stone decay. Salts cause damage to stone in several ways. The most important is the growth of salt crystals within the

pores, fissures and cracks of a stone, which can generate stresses that are sufficient to overcome the stone's tensile strength and turn the stone to fragmented pieces. Another important decay mechanism under the general term "differential stress" includes the effects of wet/dry cycling, clay swelling, differential hygric stress, differential thermal stress, and stress from differential expansion rates of material in pores (such as salts or organic material) versus in the stone.

In connection with stone deterioration, the following are crucial research questions to be properly addressed (Doehne & Price 2010):

Why are certain types of stone much more vulnerable than other types to weathering? Why are certain salts much more damaging than others? Is damage caused mostly by relatively rare environmental events (rapid cooling, drying, or condensation) or cumulative everyday stresses (humidity cycling)? Can general agreement be achieved regarding the fundamental mechanisms of salt weathering? Can the dynamics of differential stress as it relates to environmental conditions be properly modeled? Can the stone damage process and weathering forms be accurately modeled using existing knowledge? How does the hydration of salts progress, and how are crystallization pressures sustained in situ? And, above all, how can this knowledge be helpful concerning the conservation treatments of Cultural Heritage objects?

The small amount of recession rates observed at cultural heritage sites, the complexity of the deterioration mechanisms, the unavailability of chemical data that characterize the monumental building materials on site, and the uncontrolled environmental conditions, make it necessary to setup accelerated erosion chambers for conducting specific purpose experiments, under controlled conditions using chemically characterized stone samples.

2 Related Work

Although there is much work that has be done concerning in situ studies of the physicochemical processes of stone erosion and their significance to the conservation treatments of Cultural Heritage objects, the construction of accelerated erosion chambers and the conduction of specific purpose experiments, under controlled laboratory conditions is a rather under-studied issue - see the excellent survey of E. Doehne and C. Price concerning the current research on stone decay and conservation (Doehne & Price 2010), and the state-of-the-art report of C. Schellewald *et al.* concerning the simulation of stone deterioration processes (Schellewald, Theoharis, Gebremariam & Kvittingen 2013).

Gauri, Yerrapragada, Bandyopadhyay *et al.* in a series of works (Yerrapragada, Jaynes, Chirra & Gauri 1994), (Yerrapragada, Chirra, Jaynes, Li, Bandyopadhyay & Gauri 1996) and (Gauri & Bandyopadhyay 1999) described the erosion on carbonate stones, and especially marble, under polluted and unpolluted, dry or wet environments. Given that the mechanisms of surface recession and crust creation are too complex, the authors set up chemical erosion chambers to study the effects of CO_2, SO_2 and NO_2 in dry or wet controlled conditions. They also made outdoor experiments measuring the amount of material that runs off dur-

ing rain showers and related this to the exposed sample surface allowing them to estimate the recession under rainfall. The chemical processes were modeled by the unreacted-core model, which led to the calculation of the crust deposition rate in dry environments or the surface recession rate by acid rain.

G. W. Scherer examined several important weathering processes like the thermal expansion of calcite, freeze/thaw cycles, salt crystallization along with the swelling of clay inclusions (Scherer 2006). He reviewed these weathering mechanisms and outlined which aspects remain to be solved. He concluded that salt damage is one of the most serious, but least understood, causes of stone deterioration and that the essential mechanisms that cause stresses in stone are known, but that details are not clear.

D. G. Price noted that chemical weathering usually includes the solution of stone material, the degree of which depends on the amount of water passing over the surface, the solubility of the material, and the pH value of the water (Price 1995). Considering all possible reactions of stone materials with all possibly present chemicals becomes quickly very complex. However, for some stones the chemical degradation or weathering mechanisms of particular material components are relatively well known.

The effects of ozone and NO_x on the deterioration of calcareous stone was investigated by S. W. Massey. He investigated the effects of these gases on the deterioration of different stones in chamber reactions and field works in urban and rural environments (Massey 1999).

The corrosive effects of gaseous SO_2, NO_x, O_3, HNO_3, particulate matter, and acid rainfall are the topic of C. Varotsos *et al.* , concerned with the enhanced deterioration of the cultural heritage monuments (Varotsos, Tzanis & Cracknell 2009).

A. Moropoulou *et al.* presented in (Moropoulou, Bisbikou, Torfs, van Grieken, Zezza & Macri 1998) weathering phenomena on Pentelic marbles at the Demeter Sanctuary in Elefsis, Greece. A systematic mineralogical, petrographical and chemical examination of weathered stones and crusts was performed, both in situ and in the lab, on samples taken from different parts of the monument in relation to the surface characteristics as well as to the exposure to rain, sea-salt spray and wet and dry deposition of airborne pollutants and dust.

P. Storemyr in a series of works (Storemyr 1997), (Storemyr, Wendler & Zehnder 2001) and (Storemyr 2004) presented weathering phenomena at the Nidaros cathedral in Trondheim, Norway. He noted that stones from eight quarries are used in the monument and he presented and compared the behavior in weathering and conservation of the respective stone types (soapstone and greenschist). Storemyr discussed the geology, petrography and salt content of soapstone deposits. According to Storemyr the "Grytdal" stone seems also to contribute to the formation of black gypsum crusts as the observed crusts can not be attributed to air pollutants (SO_2 and particulate matter) alone.

3 Accelerated Erosion Experiments

3.1 Evaluation Data from the Cultural Heritage Sites

For the investigation of the erosion mechanisms that contribute to the degradation of stones, we collected 3D geometric data from the two Cultural Heritage sites, the Demeter Sanctuary in Elefsis, Greece, and the Nidaros Cathedral in Trondheim, Norway. Figure 1 shows a lower resolution mesh of consecutive geometric scans that took place at Elefsis in March 2013 and October 2014. The areas of the Elefsis-column, that are marked with boxes, indicate the patches we selected for illustration of measurements and investigations (compare Figure 2).

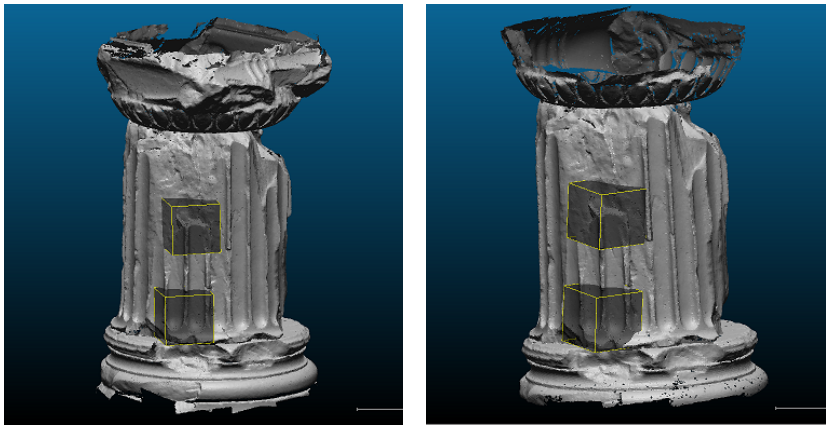

Geometric Mesh
(Round 01, 2013-03-20)

Geometric Mesh
(Round 02, 2014-10-14)

Fig. 1. Two geometric meshes of the Elefsis-column. This data was acquired in March 2013 and in October 2014. The patches that correspond to the upper box are shown in more detail in Figure 2.

At the Nidaros Cathedral several smaller areas were selected for scanning. These include two wall parts from the Lectorium (Lectorium East, with Mason Marks, and Lectorium North) and two scans from the inside of the North West and South West Tower of the Cathedral. In Figure 3 we illustrate the geometric scan of the east wall of the Lectorium that contains two mason marks. A close-up view of the areas with the mason marks is depicted in Figure 4.

The unavailability of chemical data and the small amount of recession observed at the Cultural Heritage sites themselves (Figure 5), made it necessary to complement these measurements with data obtained from accelerated erosion experiments, that study erosion parameters in isolation. Considered weathering experiments include effects that originate from polluted environments and from naturally occurring climatic conditions. The experiments that we finally decided

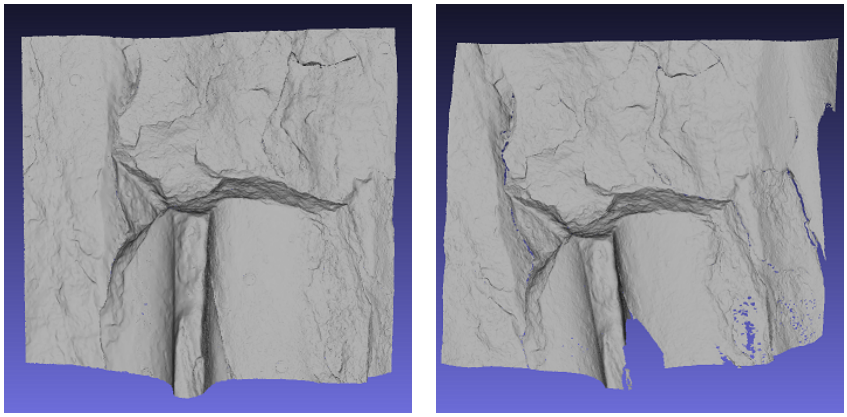

Elefsis Patch A
(Round 01, 2013-03-20).

Elefsis Patch A
(Round 02, 2014-09-24)

Fig. 2. Two Elefsis-column patches of approximately the same area of the column that was scanned at different times. Note that the shown area was scanned with high resolution.

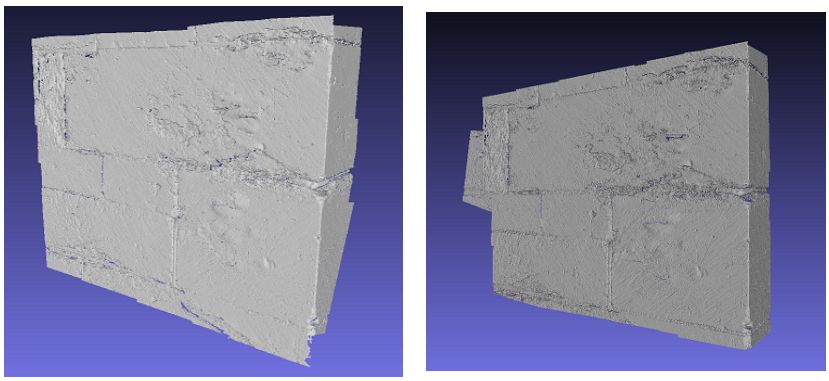

Geometric Mesh
(Round 01, 2013-04-10)

Geometric Mesh
(Round 02, 2014-09-24)

Fig. 3. Two geometric meshes of the Nidaros Cathedral. This data was acquired in April 2013 and in September 2014. The patches that show the X mason mark in more detail are shown in Figure 4

to perform, include the Salt effect (using sodium sulfate Na_2SO_4), the Freeze-and-Thaw effect, that simulate mechanical effects and two chemical experiments simulating polluted industrial environments, rich in SO_2 and NO_2 (using aqueous solutions of sulfuric acid H_2SO_4(aq) and combined sulfuric and nitric acid H_2SO_4+HNO_3(aq)).

In addition to the Salt and Freeze-and-Thaw weathering experiments, the acid weathering experiments were carried out to study the effects of polluting

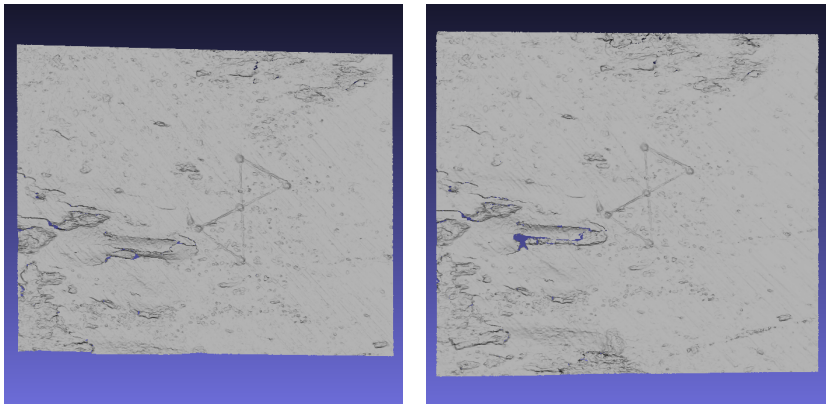

X mason mark
(Round 01, 2013-04-10)

X mason mark
(Round 02, 2014-09-24)

Fig. 4. Patches of two geometric measurement rounds showing the X mason mark that are present on the east wall of the Lectorium of the Nidaros Cathedral.

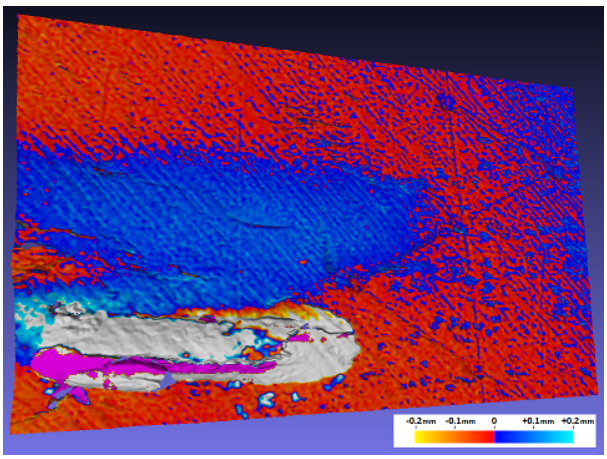

Fig. 5. Distance map of the two X mason mark patches between the two Round 01 and Round 02 3D geometry acquisitions. The meshes are at first registered, and then distances are mapped as textures onto the Round 01 mesh.

gases such as SO_2 and NO_2 in solution forms. Cyclic soaking experiments in acidic solutions of sulphuric and nitric acids, with alternating wetting and drying stages, were used to simulate the accelerated weathering. Physicochemical changes at macroscopic and microscopic levels were monitored through characterizations using multiple analytical techniques.

The experiments simulating polluted environments were performed at the Department of Chemistry at NTNU. The experiments concerning the Salt and the Freeze-and-Thaw effects were performed at the Department of Computer

and Information Science at NTNU. In the following sections we describe the constructed accelerated erosion chambers and the performed experiments for the Salt and Freeze-and-Thaw effects.

3.2 Stone Slabs and their Labeling

In this section the stone samples and the experiments carried out in our accelerated erosion chambers are briefly described. The samples are stone slabs similar to the stones used at the two Cultural Heritage sites; the Demeter Sanctuary in Elefsis, Greece, and the Nidaros Cathedral in Trondheim, Norway. Pentelic marble was used at the Demeter Sanctuary (Moropoulou et al. 1998) and Grytdal soapstone was used in the Nidaros Cathedral (Storemyr 1997). The stone slabs were named according to their origin (Elefsis, Nidaros); furthermore the soapstone slabs labelled with reference to the stone quality (Good, Bad) and finally according to their size (Large, Small) (see Figure 6). Details concerning the labeling of the specific stone samples used in each of the erosion experiments are listed in Table 3.2.

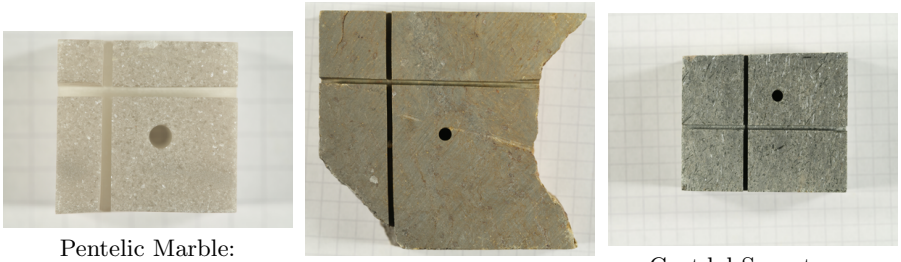

Pentelic Marble:
Elefsis Large 01

Grytdal Soapstone:
Nidaros Bad Large 01

Grytdal Soapstone:
Nidaros Good Large 01

Fig. 6. Photos of some stone slabs used in the accelerated erosion experiments.

Stone Samples			
Stone		Material	Experiment
EL1	Elefsis Large 01	*Pentelic Marble*	$Freeze - Thaw$
EL2	Elefsis Large 01	*Pentelic Marble*	*Salt*
NBL1	Nidaros Bad Large 01	*Grytdal Soapstone*	$Freeze - Thaw$
NBL2	Nidaros Bad Large 02	*Grytdal Soapstone*	*Salt*
NGL1	Nidaros Good Large 01	*Grytdal Soapstone*	$Freeze - Thaw$
NGL2	Nidaros Good Large 02	*Grytdal Soapstone*	*Salt*

Table 1. Labeling and material of stone samples

Pentelic Marble: dense metamorphic rock; homogeneous; almost entirely made of calcite (96% $CaCO_3$); with low porosity (3.64 $vol\%$) (Moropoulou et al. 1998).

Grytdal Soapstone: dense metamorphic rock; non homogeneous; made mostly of chlorite ($20\% - 60\%$) and talc ($5\% - 20\%$); with low porosity (3.60 $vol\%$) (Storemyr 1997).

3.3 Salt and Freeze-and-Thaw Chambers

In order to investigate the Salt effect, using Na_2SO_4 decahydrate, and the Freeze-and-Thaw effect we designed two erosion chambers. Figure 7 shows the Salt Chamber and the Freeze-and-Thaw Chamber which we constructed for our accelerated erosion experiments. They are controlled by Arduino micro-controllers (Arduino LLC 2015) and continuous measurements are taken over USB connections. Typical curves that originate from 24 hour measurements from both chambers are shown in Figure 12.

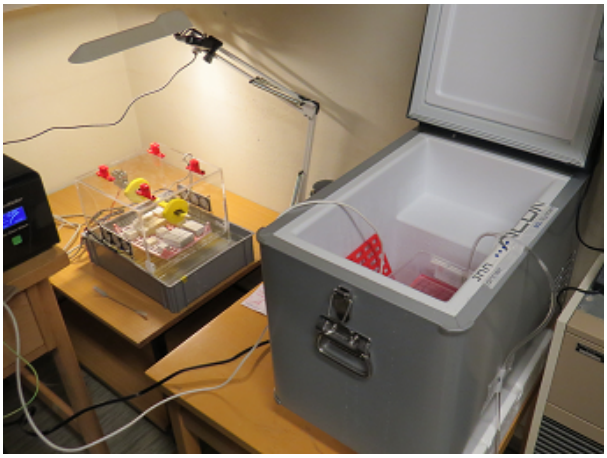

Fig. 7. The two erosion chambers (Salt and Freeze-and-Thaw) beside each other at the beginning of the second accelerated erosion round. They are located in a dedicated room for our experiments within the cellar of the Department of Computer and Information Science building at NTNU.

One cycle within the Salt Chamber takes 6 hours and consists of submerging the stones in the salt solution for 3 hours and drying them for 3 hours in a constant light airflow created by small fans attached to the chamber. Note that 3 hours is the amount of time taken for the chambers to enter into a steady state of humidity variation. Figure 8 shows the Salt Chamber in both states. The left image shows the stones lifted up. The white crust indicates that the stones already dried for a while. On the right image, the stones are submerged within

the salt solution. The temperature and humidity of the chamber is continuously monitored over the lifetime of the experiments. Diagrammatic representation of the Salt Chamber is depicted in Figure 9.

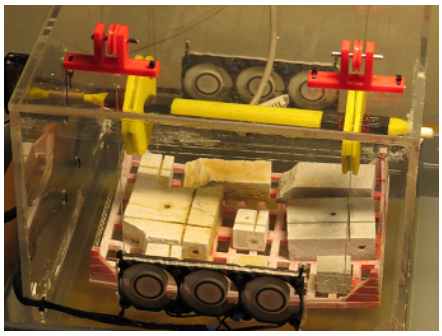

Salt Chamber
with stones being dried
(Dry phase)

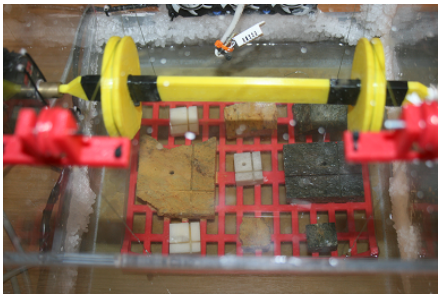

Salt Chamber
with stones submerged
(Wet phase)

Fig. 8. The Salt Chamber shown at two different cycles and states. Dry and wet phases change every three hours during the accelerated erosion cycles.

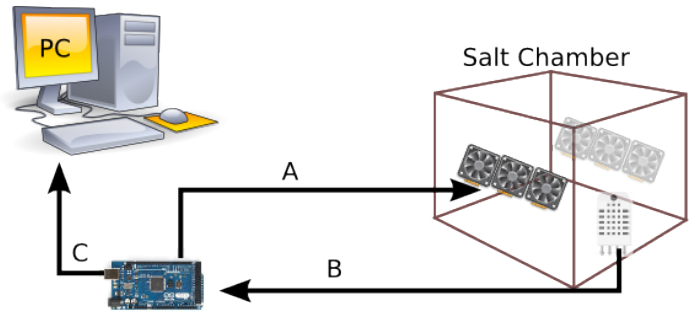

Fig. 9. Depiction of Salt Chamber control diagram: (A) Control stone submersion and fan activation; (B) Humidity and temperature reading; and (C) Data logging.

The Freeze-and-Thaw Chamber is constructed out of a small refrigerator and a water purification system that are both controlled by an Arduino microcontroller. Diagrammatic representation of the Freeze-and-Thaw Chamber is depicted in Figure 11. One cycle within the Freeze-and-Thaw Chamber takes 8 hours. This includes 3 hours of freezing and 5 hours of warming up. The length of the warm cycle was selected so that the chamber reaches a temperature of

about $5°C$. The freezing cycle guarantees a long state where the temperature is below $-5°C$. Within the last 30 minutes of the warming phase, purified water drops onto the stones. For this chamber we used a separate Arduino for continuously measuring the temperature.

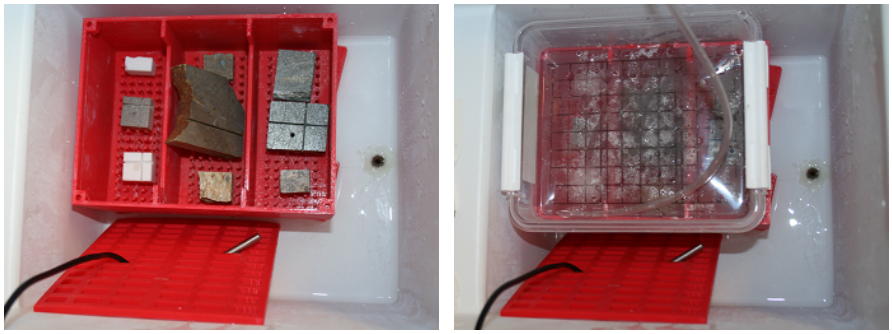

Freeze-and-Thaw Chamber stone compartments (uncovered)

Freeze-and-Thaw Chamber stone compartments (covered with rain basin)

Fig. 10. The inner structure of the Freeze-Thaw Chamber. Before a freezing cycle starts, purified water drops for 30 minutes onto the stones, simulating rain.

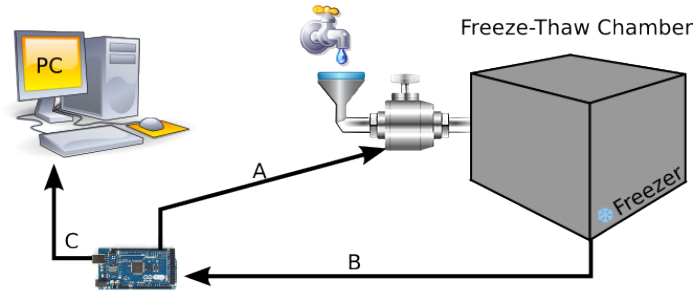

Fig. 11. Depiction of Freeze-and-Thaw Chamber control diagram: (A) Control valve for injection of purified water; (B) Temperature Readings; and (C) Data logging.

3.4 Experimental Setup

The first round of accelerated Salt effect erosion started on 19th September 2014 and was stopped on 21st October 2014, while the first round of the accelerated Freeze-and-Thaw erosion started on the 10th of November 2014 and ended on

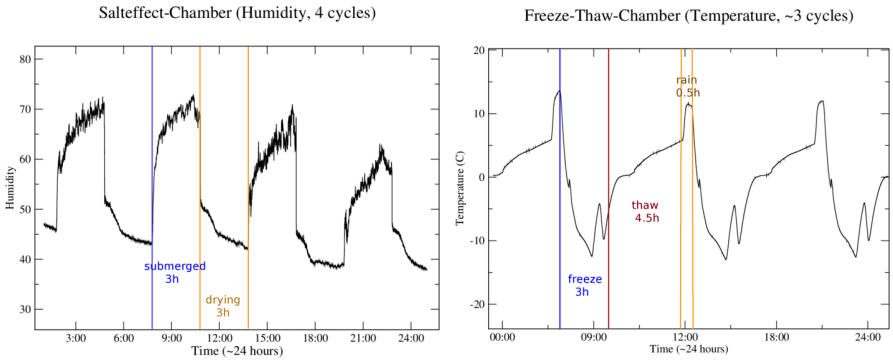

Salt Chamber: Humidity data (2014-10-14)

Freeze-and-Thaw Chamber: Temperature data (2014-11-20)

Fig. 12. Typical measurements gathered during the accelerated erosion experiments in the Salt and Freeze-and-Thaw Chambers.

the 4th of December 2014. The second round for both effects started on the 4th of March 2015. We stopped the Salt Chamber on the 20th of March 2015 for characterization of the samples taking into account the noted fast progress of the salt effect. The second round of the Freeze-and-Thaw Chamber ended on the 28th of March 2015. Erosion cycles take place between measurement cycles (see Section 3.5). Details concerning the erosion rounds of our physical chamber experiments are listed in Table 2 and Table 3.

Experiment	**Salt Chamber (Round 01)**
Start	2014-09-19 19:45
End	2014-10-21 15:52
Duration	31.83 Days (2750815 *sec*)
One cycle	21615 *sec* (submerge: 10810 *s* - drying: 10805 *s*)
Number of cycles	127.5 (128.0 taking the last drying into account)
Experiment	**Salt Chamber (Round 02)**
Start	2015-03-04 13:03
End	2015-03-20 13:19
Duration	16.01 Days (1383360 *sec*)
One cycle	21615 *sec* (submerge: 10810 *s* - drying: 10805 *s*)
Number of cycles	64.0

Table 2. Salt Chamber: Summary of the duration of the first two rounds of accelerated erosion.

Experiment	**Freeze-and-Thaw Chamber (Round 01)**
Start	2014-11-10 14:58
End	2014-12-04 15:02
Duration	24.003 Days (2073853 *sec*)
One cycle	28800 *sec* (warming up: 18000 *s* (incl. 1800 *s* rain) - freezer on: 10800 *s*)
Number of cycles	72
Experiment	**Freeze-and-Thaw Chamber (Round 02)**
Start	2015-03-04 14:25
End	2015-03-28 14:29
Duration	24.003 Days (2073853 *sec*)
One cycle	28800 *sec* (warming up: 18000 *s* (incl. 1800 *s* rain) - freezer on: 10800 *s*)
Number of cycles	72

Table 3. Freeze-and-Thaw Chamber: Summary of the duration of the first two rounds of accelerated erosion.

3.5 Measurement modalities

Several measurement techniques are used to characterize the changes that occur on the stone samples during the accelerated erosion cycles. The measurements consist of mass measurements, 3D Geometric Scans, Quantitative Evaluation of Minerals by SCANning electron microscopy (QEMSCAN), Scanning Electron Microscopy with X-ray microanalysis (SEM-EDS), 3D microscopy, micro Computed Tomography (micro-CT), X-Ray Diffraction (XRD) and Petrography. The data sets currently collected from these measurements along with some examples of the data for illustration purposes are summarized below.

3D Geometry Scans The 3D scans of the stone slabs in high resolution surface meshes of the 3D geometry of the stones, were performed by Aicon – our industrial partner in the PRESIOUS project – using a Breuckmann Scanner (AICON 3D systems 2015). An example of the resulting mesh data is depicted in Figure 13.

QEMSCAN Quantitative Evaluation of Minerals by SCANning electron microscopy is a technique that uses a Scanning Electron Microscope (SEM) combined with X-ray spectroscopy and a database to obtain accurate mineral maps for a measured stone surface, performed by Robertson CGG (Robertson CGG 2015). The results of the QEMSCAN of the stone slabs from the Freeze-and-Thaw experiment is shown in Figure 14. The used color codes and labeling of the mineral map is shown in Figure 15.

micro-CT Micro computed tomography is a technique similar to the well known CT scans performed in medicine. It provides x-ray images in 3D for small scale objects at a high resolution. It provides density information about the inner

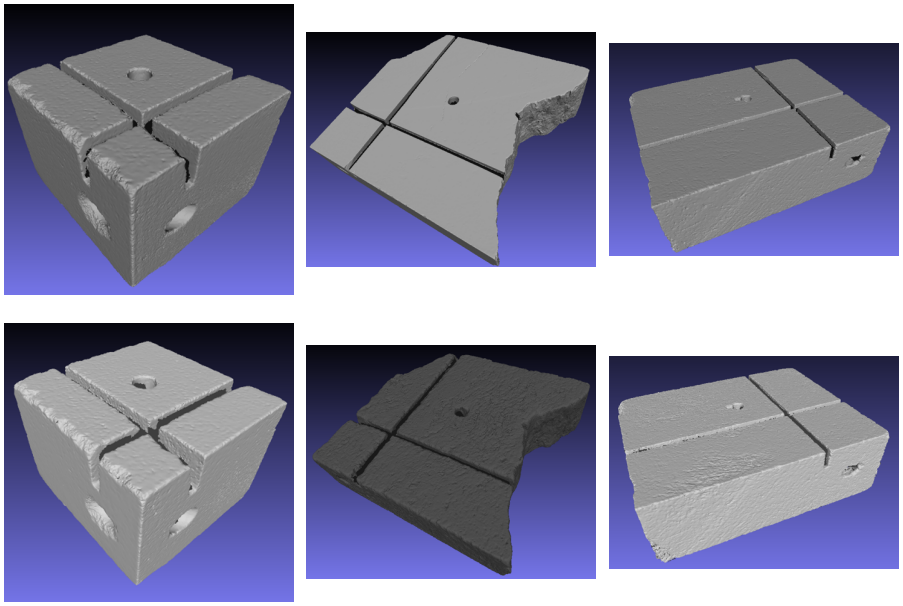

Pentelic Marble: Elefsis Large 02 | Grytdal Soapstone: Nidaros Bad Large 02 | Grytdal Soapstone: Nidaros Good Large 02

Fig. 13. Depiction of the 3D scans of some stone slabs: **Top row:** Round 01 (2014-06-02), **Bottom row:** Round 02 (2015-01-12). Notice the roughness of the surface of the R02 scans due to the erosion.

structure of the stone material and could be helpful when analyzing the 3D pore structure and volume changes of the stones. Figure 16 shows a slice from the micro-CT data acquired for the "Nidaros Bad Large 2" stone slab.

3D Microscopy To allow for additional measurements on the surface of the eroded stone slabs, 3D microscopy was employed and provides textural and 3D structure of the measured stone surfaces. Illustrations for this type of measurement are given in Figure 17 where the data of three different stone surfaces is shown. A limitation of this data is that only the depth field of the surface can be measured and that any concavities that might be present are not acquired.

Petrography Petrography is a method used since the mid 1800's for describing the mineral content and the textural relationships within rocks. A thin transparent slab slice of the stone is observed with a light microscope under plane polarised light of different orientations. Fluorescence microscopy was also used to characterize mineral contents, the porosity, fissures and cracking structures. An example for the obtained data of the Nidaros Good stone type is shown in Figure 18.

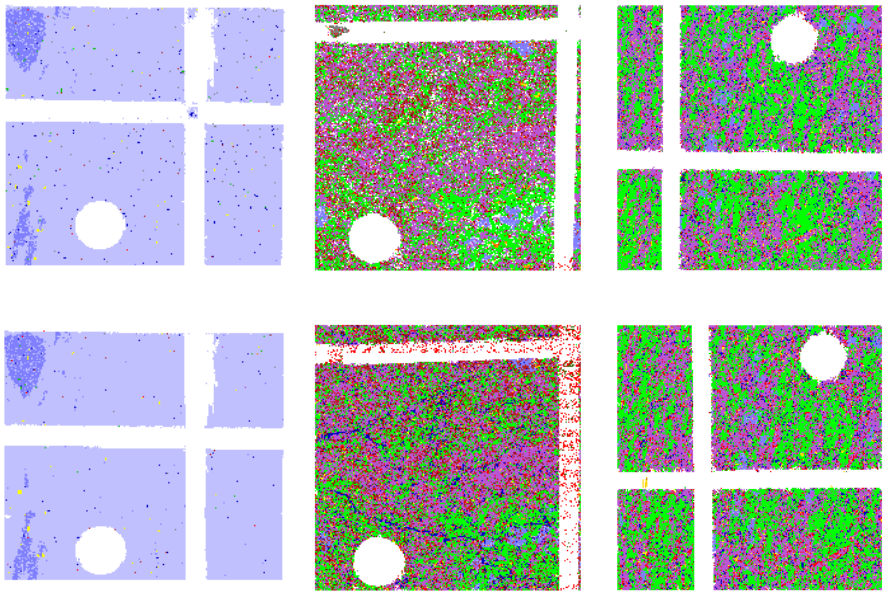

Pentelic Marble: Elefsis Large 01 | Grytdal Soapstone: Nidaros Bad Large 01 | Grytdal Soapstone: Nidaros Good Large 01

Fig. 14. Depiction of the mineral maps from the QEMSCAN of some stone slabs: **Top row:** Round 01 (2014-06-02), **Bottom row:** Round 02 (2015-01-12).

Minerals	Color	RGB-dec		
Quartz		255	255	0
K-Feldspar		221	160	221
Plagioclase Feldspar		255	105	180
Biotite		128	0	0
Illite		0	192	0
Chlorite		0	255	0
Smectite		51	102	0
Kaolinite		192	64	0
Glauconite		128	128	0
Calcite		192	192	255
Dolomite		128	128	255
Ankerite		255	192	128
Siderite		255	128	0
Gypsum/Anhydrite		178	34	34
Pyrite		255	215	0
Heavy Minerals		255	0	0
Altered Mafics		186	85	211
Pores		0	0	192
Others		128	128	128
No measurement		255	255	255

Fig. 15. Color codes of minerals that appear in the QEMSCAN mineral maps of Figure 14.

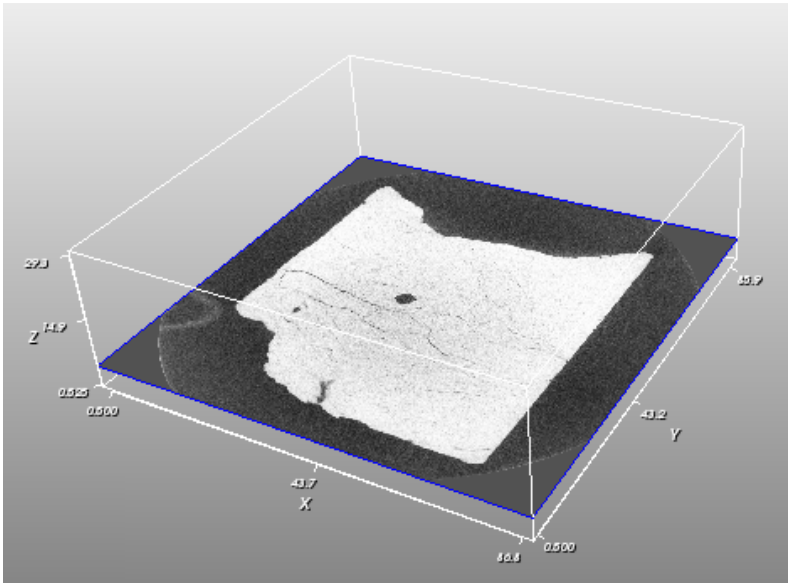

Fig. 16. Depiction of a slice from the micro-CT data of "Nidaros Bad Large 2" stone slab.

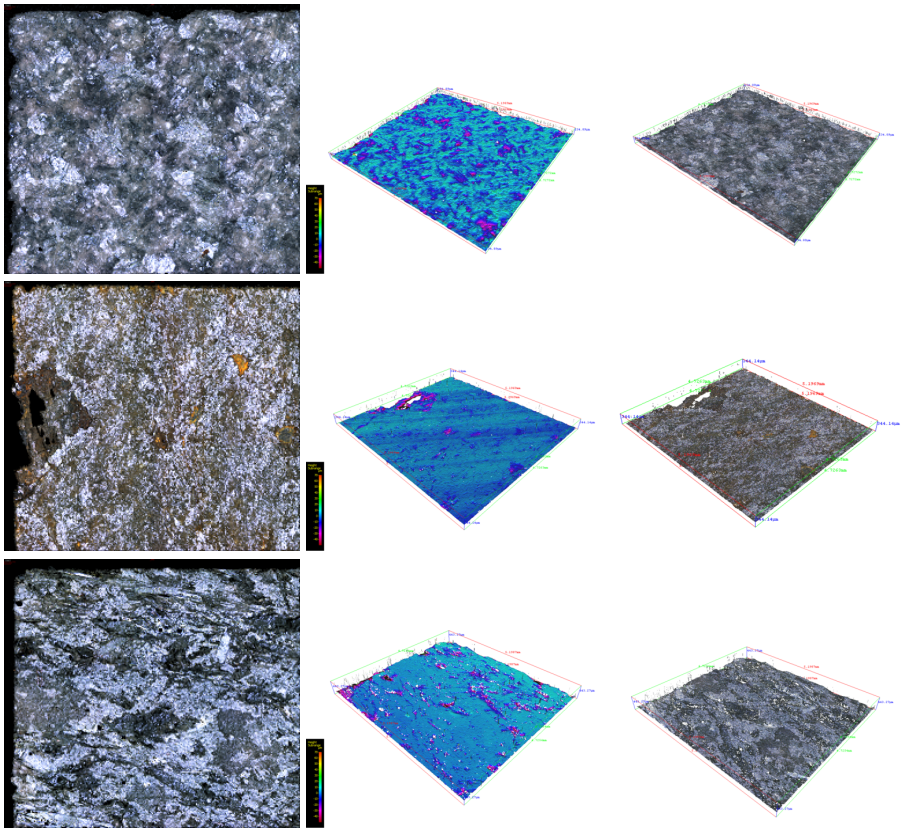

Fig. 17. 3D Microscopy images provide surface geometry data along with textural information of the scanned area. Examples from the three stone types are shown: **Top row:** Elefsis Large 01, **Middle row:** Nidaros Bad Large 01 **Bottom row:** Nidaros Good Large 01.

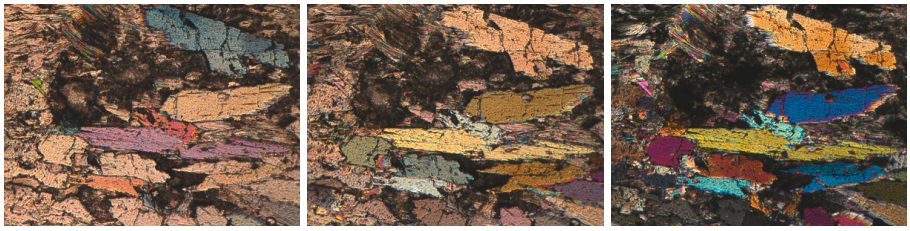

Fig. 18. A thin stone slice (Nidaros Good) is illuminated with polarized light (crossed polar in this case) that shines through it with different orientations. Depending on the orientation of the polarized light, distinctive crystals of the stone become apparent in different color shadings.

4 Results

4.1 Estimation of the extent of erosion between Erosion Cycles

Mass measurements After removal of the samples from the Salt Chamber, the stone samples were rinsed thoroughly with deionized water, dried for 24 hours at $105°C$ and cooled to room temperature in a desiccator before mass measurements. The same procedure, except rinsing with deionized water, was followed for the stone samples from the Freeze-and-Thaw Chamber.

Mass Loss Δm (gr)					
Stone		m_1 gr	m_2 gr	Δm gr	$\Delta m/m$ %
EL1	$Freeze-Thaw$	29.1283	29.0847	-0.0436	-0.15
EL2	$Salt$	25.0409	24.8459	-0.1950	-0.78
NBL1	$Freeze-Thaw$	169.2780	168.8975	-0.3805	-0.22
NBL2	$Salt$	195.8884	188.9025	-6.9859	-3.57
NGL1	$Freeze-Thaw$	101.7920	101.7464	-0.0456	-0.04
NGL2	$Salt$	161.2788	160.5487	-0.7301	-0.45

Table 4. Measurements of the mass loss for the different stone slabs. m_1 initial mass, m_2 mass after 1^{st} erosion cycle.

Mass measurements confirm our observation that stones from Nidaros (i.e. NBL1 and NBL2) suffer more erosion than the other stones and also that the Salt effects are more dramatic than the Freeze-Thaw effects (see Table 4.1).

Estimating erosion using micro-CT scans One way of estimating the mean erosion δ is to assume that the erosion takes place equally on all faces of the slab and that the slab can be approximated as a cube with edge length h (*"Cubic Volume Approximation"*). Then $\delta = \frac{1}{2}\Delta h$.

Thus, for estimating Δh we use the volumes V_1 and V_2 of the slab before and after erosion respectively. Then Δh is computed from the slab volumes as $\Delta h = \sqrt[3]{V_2} - \sqrt[3]{V_1} = h_2 - h_1$, where h_1 and h_2 represent the cube edge lengths before and after the erosion cycle respectively. The volumes V_1 and V_2 were computed using non-void voxel counting on the micro-CT scans of the slabs.

Estimating erosion using micro-CT scans and surface scans A second way of estimating δ is to use the surface areas S_1 and S_2 of the mesh before and after erosion respectively (*"Surface Area Approximation"*). Assuming that the surface area doesn't change too much we can use the differential equation $\Delta V = S\Delta h$, and $\delta = \Delta h = \Delta V/S$, where $\Delta V = V_2 - V_1$ and $S = S_{avg} = (S_1 + S_2)/2$. The surface areas S were computed using the summation of the

triangles area of the scanned mesh. Since the micro-CT data did in some cases not cover the whole volume of the slabs (in particular the larger stone slabs did not fit into the measurement space) during the first round (R01) measurements, V_1 could not be directly computed from them, so finally it was computed from the first round mass m_1 using the second round density ρ_2, which was considered constant between the two cycles.

Note that the above two ways of estimating δ are based on different measurements (3D scans and micro-CT). We have estimated δ using both methods and since the results for the various slabs are quite close to each other, the validity of our approximation is confirmed (see Table 4.1).

Mean Erosion δ (mm)							
Stone		V_1 cm^3	V_2 cm^3	ΔV cm^3	S cm^2	$\delta^{(a)}$ mm	$\delta^{(b)}$ mm
EL1	$Freeze-Thaw$	10.8250	10.7281	-0.0969	31.3598	-0.0331	-0.0309
EL2	$Salt$	9.3050	9.1773	-0.1277	28.3975	-0.0483	-0.0450
NBL1	$Freeze-Thaw$	$^{(*)}$61.9314	61.7922	-0.1392	120.5537	-0.0148	-0.0115
NBL2	$Salt$	70.3382	68.6979	-1.6403	126.5692	-0.1617	-0.1296
NGL1	$Freeze-Thaw$	$^{(*)}$35.4548	35.4389	-0.0159	72.1983	-0.0025	-0.0022
NGL2	$Salt$	$^{(*)}$55.5347	55.2833	-0.2514	102.9147	-0.0288	-0.0244

Table 5. Computation of the mean erosion for the different stone slabs: (a) Cubic volume approximation; and (b) Surface area approximation. $^{(*)}$ Volume V_1 computed from mass m_1 using density ρ_2 considered constant.

Estimating erosion on every vertex of the stone mesh A key problem in measuring erosion based on scans made across time is the difficulty in registering these scans. Due to the absence of an external reference frame, a typical registration algorithm, such as Iterative Closest Point (ICP) (Besl & McKay 1992), will align the scans so as to minimise the RMS error between them, which is not an ideal solution in case of erosion, since it diminishes the common erosion that has to be measured (see Figure 19 (a)). Here is how we handled this problem in the case of the erosion chamber slabs.

We first register the top surface of the slabs using ICP and assume that this registration is sufficient in terms of the X and Y dimensions that define the top surface. The question is by how much to displace the slab in Z in order to accurately describe the erosion effect, see Figure 19 (b). Let us call this necessary displacement ΔZ. This should be equal to the computed mean erosion δ.

Consider two point sets $M = \{\mathbf{m}_1, \mathbf{m}_2, \ldots, \mathbf{m}_p\}$, that represents the initial surface of a stone, and $T = \{\mathbf{t}_1, \mathbf{t}_2, \ldots, \mathbf{t}_q\}$ that represents the weathered surface of the same stone, where $\mathbf{m}_i,\ \mathbf{t}_j \in \mathbb{R}^3$.

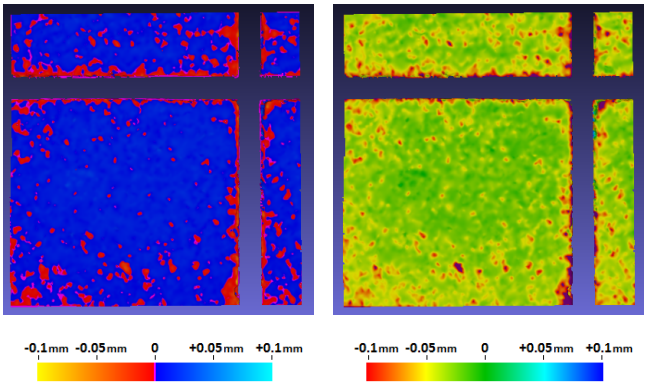

(a) (b)

Fig. 19. Differential Map of initial to eroded mesh for the frontal surface of the stone slab Elefsis Large 3 (EL3): (a) Slabs registered using ICP (blue indicates positive distances and red indicates negative distances); and (b) Slabs displaced in Z using estimated erosion value (red indicates most eroded areas and blue least eroded areas). Colors are mapped in the interval of $[-0.1mm \sim +0.1mm]$.

The distance $d_e(\mathbf{m}_i) = \min_j(\|\mathbf{m}_i - \mathbf{t}_j\|)$ can be used as a local erosion measure which expresses at each vertex of the initial model M the distance of the closest vertex of the eroded model T, and is a scalar mapping of the erosion measure at each vertex of the initial stone model M, to which the eroded model T is registered. $\|\mathbf{m}_i - \mathbf{t}_j\|$ is the Euclidean distance of a point of M from a point of T.

Figure 19 depicts the distance maps (i.e. the $d_e(\mathbf{m}_i)$) between round 01 and 02 meshes of Elefsis Large 3, and consequently the computed erosion measure textured on the initial mesh.

4.2 Physico-chemical aspects of the erosion

The physico-chemical aspects of the erosion involves geometrical information and physicochemical data on the surface of the object being eroded. A crucial first step for this procedure is the registration of the acquired geometric mesh data with the QEMSCAN mineral map texture data (Figures 20 and 21).

The general registration transformation matches landmark points annotated on the geometry image of the scanned 3D mesh, and the corresponding landmark points annotated on the QEMSCAN texture, which are considered as the invariant reference points under the correspondence transformation. These points are localized using the hole and the cross which are engraved onto the slabs for this purpose.

Estimating Mineral Composition using the QEMSCAN data One way of estimating the mineral composition of each stone is by computing the occur-

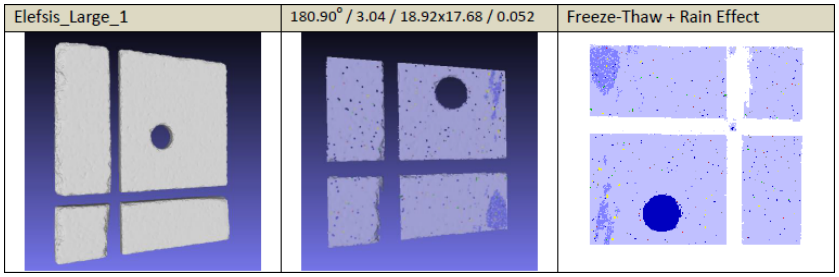

Fig. 20. Depiction of geometry and QEMSCAN registration results for the Elefsis Large 1 (EL1) marble slab.

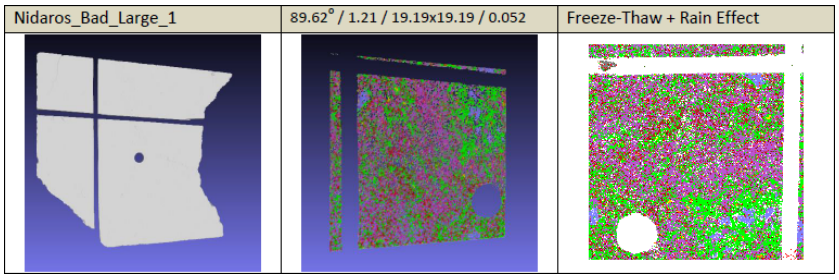

Fig. 21. Depiction of geometry and QEMSCAN registration results for the Nidaros Bad Large 1 (NBL1) soapstone slab.

Minerals	**EL1**		**EL2**		**NBL1**		**NBL2**		**NGL1**		**NGL2**	
% v/v	R01	R02	R01	R02	R01	R02	R01	R02	R01	R02	R01	R02
Quartz	0.21	0.17	0.03	0.01	1.27	1.42	1.71	0.71	1.90	1.48	2.22	1.83
K-Feldspar	-	-	-	-	-	-	-	-	-	-	-	-
P-Feldspar	0.00	0.00	0.00	0.00	0.01	0.00	0.00	0.00	0.00	0.00	0.00	0.00
Biotite	0.00	0.00	0.00	0.00	4.55	4.98	4.20	2.75	1.22	1.91	1.50	1.18
Illite	0.10	0.05	0.46	0.37	0.00	0.00	0.00	0.00	0.00	0.00	0.00	0.00
Chlorite	0.01	0.00	0.00	0.01	31.35	29.19	31.23	11.82	39.09	37.69	18.84	12.95
Smectite	0.00	0.00	0.00	0.00	0.94	0.94	0.74	0.37	0.46	0.46	0.76	0.98
Kaolinite	-	-	-	-	-	-	-	-	-	-	-	-
Glauconite	-	-	-	-	-	-	-	-	-	-	-	-
Calcite	93.89	89.86	98.06	97.07	0.21	0.20	0.00	0.04	0.32	0.16	0.52	0.65
Dolomite	4.13	4.28	0.20	0.42	2.34	1.62	0.13	0.17	2.85	2.54	9.67	8.85
Ankerite	-	-	-	-	-	-	-	-	-	-	-	-
Siderite	0.00	0.00	0.00	0.00	0.36	0.53	0.26	1.24	0.14	0.11	0.06	0.40
Gypsum	0.08	0.05	0.06	0.40	7.31	10.24	3.86	7.16	0.02	0.10	0.03	4.24
Pyrite	0.00	0.00	0.01	0.03	0.30	0.18	1.24	0.57	0.23	0.25	0.13	0.34
H-Minerals	0.02	0.02	0.03	0.01	5.93	6.76	5.30	6.71	4.51	7.23	5.18	6.41
Alt-Mafics	0.00	0.01	0.00	0.02	40.20	34.16	40.82	32.66	42.98	38.55	56.89	48.81
Pores/Void	1.32	5.52	1.14	1.62	3.18	6.65	2.34	30.62	5.70	5.76	3.81	9.39
Others	0.25	0.02	0.36	0.77	2.06	2.93	8.18	5.17	0.58	3.74	0.37	3.97

Table 6. Surface coverage (% v/v composition) of the minerals that appear in the mineral maps of the various stone slabs for the two measurement rounds R01 and R02.

rences of each mineral on the QEMSCAN textures. This gives the relative surface coverage for each mineral which is actually related to the volume composition of each stone % v/v (see Table 6).

5 Concluding remarks

Although the interpretation of the results from the accelerated weathering experiments on the marble and soapstone at macroscopic and microscopic levels is still in progress, we can infer that the investigation conducted has given an insight into the changes occurring during erosion/weathering of these stones.

Low-cost, small scale, automated weathering chambers for studying accelerated Salt and Freeze-and-Thaw effects on stones were successfully designed, constructed and used. The weathered stone samples were exhaustively characterized by employing a wide range of analytical techniques and approaches that have provided valuable information on the weathering processes and mechanisms.

6 Acknowledgments

This research is part of the PRESIOUS project and has received funding from the European Unions Seventh Framework Programme STREP Project under grant agreement no 600533.

References

AICON 3D systems (2015), 'http://aicon3d.com/start.html'.

Arduino LLC (2015), 'http://www.arduino.cc/'.

Besl, P. J. & McKay, N. D. (1992), 'A method for registration of 3-D shapes', *IEEE Trans. Pattern Anal. Mach. Intell.* **14**(2), 239–256.

Doehne, E. & Price, C. A. (2010), Stone conservation: An overview of current research, Technical report, Getty Conservation Institute, Los Angeles, US.

Gauri, K. L. & Bandyopadhyay, J. K. (1999), *Carbonate Stone, Chemical Behaviour, Durability and Conservation*, John Wiley & Sons, Inc.

Massey, S. (1999), 'The effects of ozone and {NOx} on the deterioration of calcareous stone', *Science of The Total Environment* **227**(2–3), 109–121.

Moropoulou, A., Bisbikou, K., Torfs, K., van Grieken, R., Zezza, F. & Macri, F. (1998), 'Origin and growth of weathering crusts on ancient marbles in industrial atmosphere', *Atmospheric Environment* **32**(6), 967–982.

Price, D. G. (1995), 'Weathering and weathering processes', *Quarterly Journal of Engineering Geology and Hydrogeology* **28**(3), 243–252.

Robertson CGG (2015), 'http://www.robertson-cgg.com/'.

Schellewald, C., Theoharis, T., Gebremariam, K. F. & Kvittingen, L. (2013), State of the art report on deterioration simulation, Technical Report PRESIOUS-D3.1, NTNU, Trondheim, Norway.

Scherer, G. (2006), Internal stress and cracking in stone and masonry, *in* M. KONSTAGDOUTOS, ed., 'Measuring, Monitoring and Modeling Concrete Properties', Springer Netherlands, pp. 633–641.

Storemyr, P. (1997), The stones of Nidaros: an applied weathering study of Europe's northernmost medieval cathedral, PhD thesis, Norwegian University of Science and Technology (NTNU).

Storemyr, P. (2004), 'Weathering of soapstone in a historical perspective', *Materials Characterization* **53**, 191–207.

Storemyr, P., Wendler, E. & Zehnder, K. (2001), Weathering and conservation of soapstone and greenschist used at Nidaros Cathedral (Norway), *in* A. Lunde, Ø. & Gunnarsjaa, ed., 'Report Raphael II Nidaros Cathedral Restoration Trondheim Norway 2000.', EC Raphael Programme – European Heritage Laboratory.

Varotsos, C., Tzanis, C. & Cracknell, A. (2009), 'The enhanced deterioration of the cultural heritage monuments due to air pollution', *Environ Sci Pollut Res* **16**, 590–592.

Vergès-Belmin, V. (2008), 'Illustrated glossary on stone deterioration patterns = glossaire illustré sur les formes d' altération de la pierre', Paris: ICOMOS (International Council on Monuments and Sites) and ISCS (International Scientific Committee for Stone). English-French ed.

Yerrapragada, S., Chirra, S., Jaynes, J., Li, S., Bandyopadhyay, J. & Gauri, K. (1996), 'Weathering rates of marble in laboratory and outdoor conditions', *Journal of Environmental Engineering* **122**(9), 856–863.

Yerrapragada, S. S., Jaynes, J. H., Chirra, S. R. & Gauri, K. L. (1994), 'Rate of weathering of marble due to dry deposition of ambient sulfur and nitrogen dioxides', *Analytical Chemistry* **66**(5), 655–659.